Acta Crystallographica Section B
Structural Science
ISSN 0108-7681

How to easily replace the independent atom model – the example of bergenin, a potential anti-HIV agent of traditional Asian medicine

Birger Dittrich,[a] Manuela Weber,[b] Roman Kalinowski,[b] Simon Grabowsky,[b] Christian B. Hübschle[a] and Peter Luger[b]*

[a]Institut für Anorganische Chemie, Georg-August-Universität Göttingen, Tammanstrasse 4, D-37077 Göttingen, Germany, and [b]Institut für Chemie und Biochemie/Kristallographie, Freie Universität Berlin, Fabeckstrasse 36a, D-14195 Berlin, Germany

Correspondence e-mail: luger@chemie.fu-berlin.de

Received 9 July 2009
Accepted 2 November 2009

Bergenin, which has been isolated from a variety of tropical plants, has several pharmacological applications in traditional Asian medicine. Its electron-density distribution was obtained from a room-temperature low-resolution X-ray data set measured with point detection making use of multipole populations from the invariom library. Two refinement models were considered. In a first step, positional parameters and ADPs were refined with fixed library multipoles (model E1). This model was suitable to be input into a second refinement of multipoles (model E2), which converged smoothly although based on Cu $K\alpha$ room-temperature data. Quantitative results of a topological analysis of the electron density from both models were compared with Hartree–Fock and density-functional calculations. With respect to the independent atom model (IAM) more information can be extracted from invariom modelling, including the electrostatic potential and hydrogen-bond energies, which are highly useful, especially for biologically active compounds. The reliability of the applied invariom formalism was assessed by a comparison of bond-topological properties of sucrose, for which high-resolution multipole and invariom densities were available. Since a conventional X-ray diffraction experiment using basic equipment was combined with the easy-to-use invariom formalism, the procedure described here for bergenin illustrates how it can be routinely applied in pharmacological research.

1. Introduction

In 3 years the crystallographic community will celebrate 100 years of X-ray diffraction. Since its discovery in 1912, X-ray crystal-structure analysis has seen several stages of development. For the first 50 years, the method was applicable only in exceptional cases and with almost unacceptable effort, so that for example the Cambridge Crystallographic Database (CSD; Allen, 2002) lists less than 1000 organic and organometallic crystal structures published before 1960.

Through simultaneous developments in solving the phase problem, the introduction of automatic diffractometers and progress in computer technology, the number of published crystal structures increased dramatically, as illustrated by the number of CSD entries now being close to half a million. In almost all cases the IAM was applied that uses spherical scattering factors, which do not allow a detailed description of chemical bonding. However, a deeper understanding of the chemistry of a given compound can only be achieved by taking into account non-spherical valence electron density.

For aspherical-atom modelling, the Hansen & Coppens multipole formalism (Hansen & Coppens, 1978) is commonly used. It is a pseudoatom formalism (Stewart, 1976) that

Table 1
Crystallographic data and IAM refinement.

Crystal data	
Chemical formula	$C_{14}H_{16}O_9 \cdot H_2O$
M_r	346.28
Crystal system, space group	Orthorhombic, $P2_12_12_1$
Temperature (K)	293
a, b, c (Å)	7.488 (1), 13.934 (1), 14.275 (1)
V (Å^3)	1489.4 (2)
Z	4
Radiation type	Cu $K\alpha$
μ (mm^{-1})	1.16
Crystal size (mm)	0.50 × 0.38 × 0.36
Data collection	
Diffractometer	Stoe four-circle, point detector
Absorption correction	None
No. of measured, independent and observed $I > 2\sigma(I)$ reflections	5547, 2531, 2467
R_{int}, R_{sigma}	0.019, 0.018
Overall completeness (%)	100
Redundancy	2.2
IAM refinement	
Refinement on	F^2
$R_1[F > 4\sigma(F)]$, $wR_2(F^2)$, S	0.021, 0.054, 1.07
No. of reflections	2531
No. of parameters	290
$(\Delta/\sigma)_{max}$	< 0.0001
$\Delta\rho_{max}$, $\Delta\rho_{min}$ (e Å^{-3})	−0.11/0.13
Flack parameter	−0.02 (12)

describes the asphericity of an atomic electron density by a sum of spherical harmonic-density functions. The application of a multipole model may require up to 30 additional parameters per atom and therefore makes the collection of high-resolution diffraction data ($d \leq 0.5$ Å) necessary in order to obtain a high data-to-parameter ratio. Such a resolution is generally far beyond the scattering power of macromolecules and needs considerable experimental effort even in small-molecule crystallography, so that some limitations in this field still exist.

Recently, the maximum entropy method (MEM) has been used in a number of cases (van Smaalen *et al.*, 2003; Hofmann, Kalinowski *et al.*, 2007; Hofmann, Netzel & van Smaalen, 2007; Netzel *et al.*, 2008) as an alternative to the multipole model. Since MEM also requires high-order data, the experimental challenge still remains.

To overcome the limitations mentioned above, various activities have been initiated in the last few years to establish databases of aspherical scattering factors obtained either from experimental or theoretical investigations (Pichon-Pesme *et al.*, 1995; Zarychta *et al.*, 2007; Dominiak *et al.*, 2007). One concept is to replace the IAM by the invariom formalism (Dittrich *et al.*, 2004), an aspherical scattering model which assigns fixed multipoles to each atom of a structure from an invariom library to calculate non-spherical scattering factors. This allows the refinement of only positional and displacement parameters as in an IAM refinement, so that data sets of medium resolution ($d \leq 0.9$ Å) are sufficient. Application of the invariom method was made possible by easy-to-use software that has been developed recently, see Fig. 1 (Dittrich *et al.*, 2005; Hübschle *et al.*, 2007). At present the invariom library, which is under continuous development, contains all entries for amino acids/oligopeptides, some entries for nucleotide bases/nucleosides and a large number of entries for organic molecules, *e.g.* carbohydrates. An extension to common inorganic molecules is planned. Since the requirements for X-ray and computer equipment are modest, the aspherical invariom model lends itself to a wide application including cases where crystal scattering power might limit the attainable resolution or if the latest equipment is not available.

This is demonstrated by the example of bergenin (Frick *et al.*, 1991), a compound of traditional Asian medicine, which has been isolated from a variety of tropical plants. It is known for *anti*-HIV and other biological activities (Ye *et al.*, 2004).

2. Bergenin structure, X-ray experiments

The X-ray structure of bergenin monohydrate is well documented. Two room-temperature structures (Shang-Zhen *et al.*, 1989; Ye *et al.*, 2004) and one 120 K study were reported (Caldas *et al.*, 2002). In addition, the X-ray structure of the corresponding penta-acetate is known (Frick *et al.*, 1991). The molecular structure of bergenin consists of a tricyclic system, a D-glucopyranose ring in $^4C_1$ conformation, an annelated δ-lactone ring and an aromatic ring fused to the lactone ring (Fig. 2). All OH groups are involved in hydrogen bonds, one is intramolecular and six are intermolecular (for details see below). The absolute structure assigned in this study is the same as was established by chemical preparative work on bergenin where it was obtained from an α-D-glucopyranosyl bromide (Frick *et al.*, 1991). The sample used in this study was kindly provided by Dr Tran Dinh Thang from Vinh University, Vinh City, Vietnam.

To demonstrate that inexpensive experimental equipment which is far from today's standard is sufficient for the required data collection, the X-ray intensities were measured with point detection on a more than 20 year-old diffractometer at room temperature with Ni-filtered Cu $K\alpha$ radiation from a sealed 2 kW tube providing a homogeneous beam diameter of

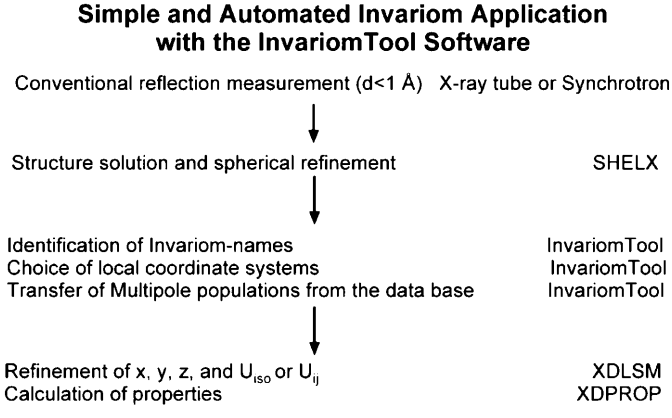

Figure 1
Scheme describing the application of the invariom formalism using the *InvariomTool* software (Hübschle *et al.*, 2007).

Table 2
Multipole refinements.

Model	E1	E2
No. of reflections in refinement	2436	2436
No. of parameters	289	201
Weighting scheme	$1/\sigma^2(F_o^2)$	$1/\sigma^2(F_o^2)$
R_F	0.0141	0.0130
R_w	0.0145	0.0131
$R(F^2)$	0.0315	0.0291
$wR(F^2)$	0.0286	0.0259
Gof	2.19	1.87
N_{ref}/N_{var}	8.4	12.1
(Δ/σ_{max})	$< 10^{-7}$	$< 10^{-8}$
$\Delta\rho_{max}$, $\Delta\rho_{min}$ (e Å^{-3})	−0.092/0.109	−0.087/0.093
Flack parameter	0.02 (7)	0.02 (7)

1.0 mm at the crystal site. From an exposure time of 8 d, around 5550 reflections were collected to a moderate resolution of $\sin\theta/\lambda = 0.59$ Å^{-1} ($d = 0.85$ Å). For further experimental details, see Table 1.

2.1. Invariom application, refinement and theoretical calculations

The room-temperature atomic parameters known from the literature (Ye *et al.*, 2004) were used to initiate a conventional spherical refinement with *SHELXL* (Sheldrick, 2008). Making use of the *InvariomTool* software (Hübschle *et al.*, 2007), 42 invarioms were assigned, 41 of them automatically by the software, which analyses the molecular geometry and then identifies the appropriate invariom. For one atom, user intervention was required. Because many atoms have the same chemical environment, only 19 of the 42 invarioms are unique. Input files for *XD*2006 (Volkov, Macchi *et al.*, 2006) containing the multipole population parameters and also the local atomic coordinate systems adjusted to site symmetry (if any) were automatically generated by the software. In a first refinement step (hereafter referred to as experimental model E1), only the positional and displacement parameters were refined, while the multipoles were kept fixed to the invariom library values. Hence, in this invariom refinement fixed non-spherical scattering factors were applied and the number of parameters used in *XD* was the same as in the spherical refinement, see also Table 2. It has recently been shown that a considerable improvement of anisotropic displacement parameters (ADPs) from invariom model refinement can be achieved (Dittrich *et al.*, 2005, 2008), leading to ADPs of a quality equivalent to those of a free multipole refinement. Hence multipole refinement was attempted using the converged E1 model and the invariom library multipoles as input (fixed x, y, z and ADPs). The refinement procedure of this model (referred to as experimental model E2) converged smoothly after seven cycles, the number of refined parameters was even lower than for model E1.

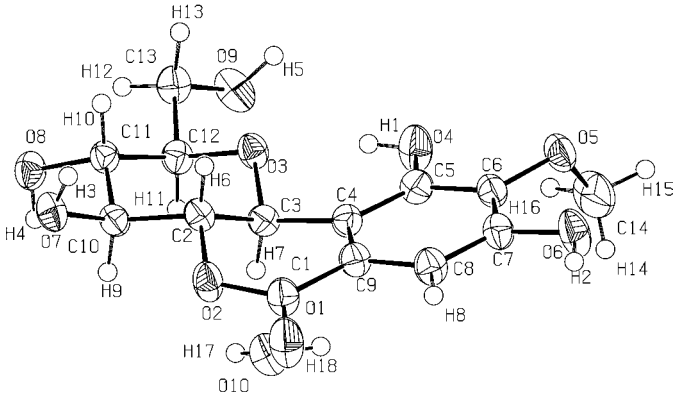

Figure 2
ORTEP (Burnett & Johnson, 1996) representation of the structure of bergenin monohydrate with atomic numbering scheme. Displacement ellipsoids are drawn at 50% probability.

Conventional figures of merit for the IAM and the two E1 and E2 refinements are summarized in Tables 1 and 2. R values decrease considerably from IAM to E1, and are further reduced from E1 to E2; this also holds for the minimum and maximum residual density. We conclude that the application of the invariom formalism provides a molecular geometry (positional parameters and ADPs) which allows a stable refinement of multipoles even from a low-resolution room-temperature data set. However, one has to be very careful and aware of parameter correlations, as recently pointed out by Dittrich *et al.* (2009).

We note that the procedure described here could be equally well applied to the 120 K data reported by Caldas *et al.* (2002).

The molecular geometry obtained from model E1 was entered into single-point calculations with HF and DFT methods [HF/6-311+G(d,p) and B3LYP/6-311+G(d,p); Frisch *et al.*, 1998] to allow a comparison with the experimental results.

The experimental (E1 and E2) and theoretical electron-density distributions were analyzed quantitatively according to Bader's Quantum Theory of Atoms in Molecules (QTAIM) formalism (Bader, 1994). For the experimental data *XDPROP* of the *XD*2006 program suite was employed and the theoretical calculations were analyzed with *AIM*2000 (Biegler-König, 2001).

3. Results and discussion

A qualitative picture of chemical bonding is illustrated in static deformation densities for a couple of selected planes for models E1 and E2 (Fig. 3). While in the intramolecular sections (aromatic ring and intramolecular HB), the densities are rather alike for E1 and E2 (with somewhat more pronounced negative regions for E2), the lone-pair density of the acceptor oxygen shows some differences in the intermolecular HB. For the E1 model, the two lobes are properly separated, while a continuous distribution is seen for the E2 model.

3.1. Atomic and bond-topological properties

As already mentioned, Bader's AIM formalism was applied to quantitatively analyze and to compare atomic and bond-topological properties.

From the electron-density distribution obtained after refinement of models E1 and E2, all expected bond-critical points (b.c.p.s) on the covalent bonds and on the hydrogen bonds were found. In addition, ring-critical points (r.c.p.s) were identified for the three six-membered rings mentioned above. Topological properties at the b.c.p.s were compared for the E1 and E2 models with the corresponding results of the two theoretical calculations at the Hartree–Fock and density-functional level. For a list of detailed data, see the supporting information.[1] The mean differences between experiment (E1 and E2) and theory (Hartree–Fock and B3LYP calculations, coded H and B) summarized in Table 3 agree satisfactorily and show a normal spread, similar to that found previously for electron-density studies based on high-resolution data sets, where inconsistencies in $\rho(\mathbf{r}_{bcp})$ and $\nabla^2\rho(\mathbf{r}_{bcp})$ of ~ 0.1 e Å^{-3} and 2–5 e Å^{-5} are tolerated (Luger, 2007; Messerschmidt *et al.*, 2005; Dittrich *et al.*, 2002; Grabowsky *et al.*, 2009). In addition, we note that the average experimental/theoretical differences are very comparable to the differences between the two theoretical calculations. There is a marginal increase of the experimental *versus* theoretical difference in $\rho(\mathbf{r}_{bcp})$ for the multipole-refinement model E2, which is not unexpected since this model might account better for the crystalline state than model E1. On the other hand, the E1–E2 differences are very small, so that with respect to bond-topological properties significant differences between the E1 and E2 models are not seen. Hence, in the following discussion we only refer to the E2 results.

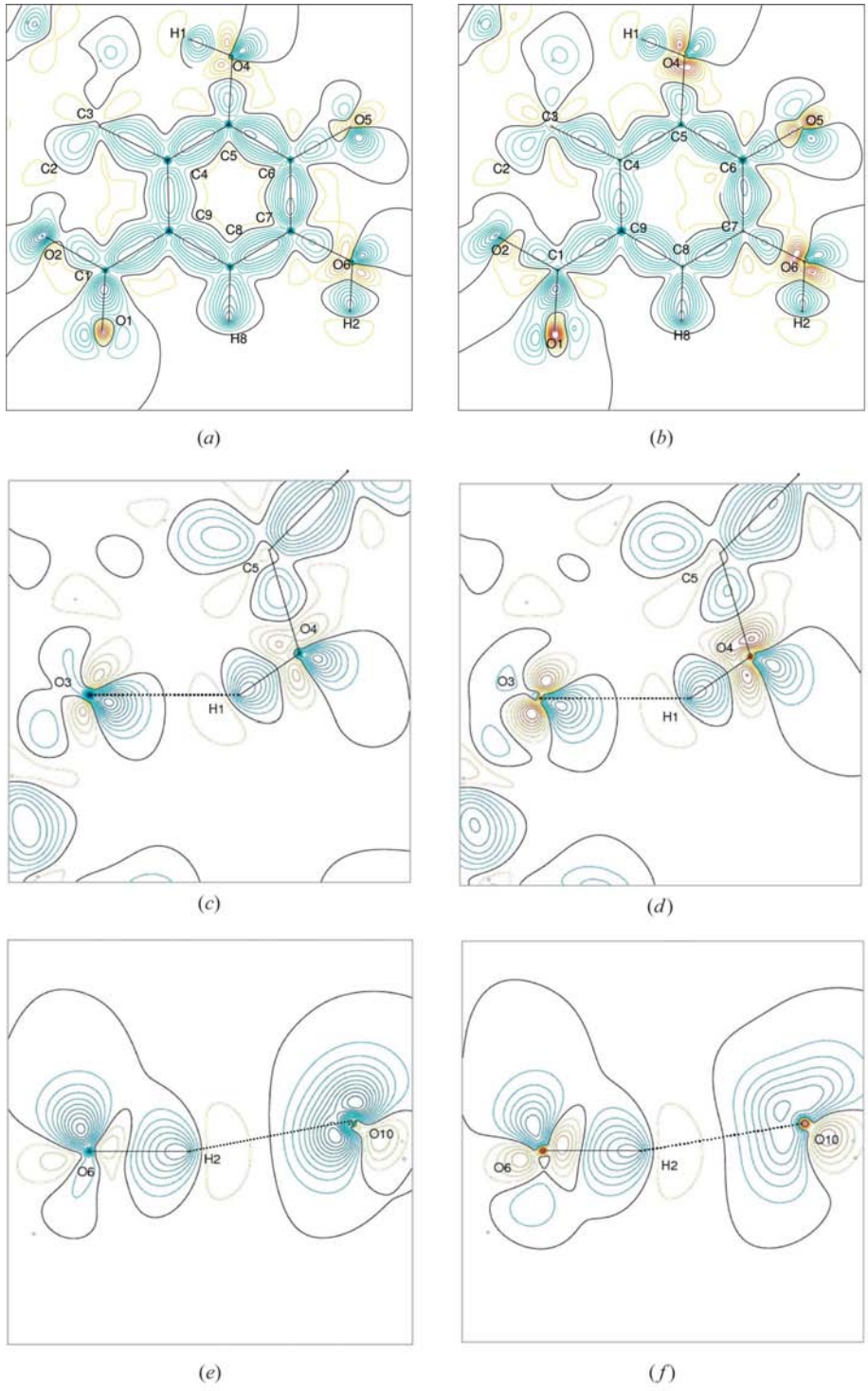

Figure 3
Static deformation-density maps in the aromatic ring (top), in the plane of the intramolecular hydrogen bond (middle) and in the plane of the strongest (intermolecular) hydrogen bond O6—H2···O10 (bottom). Left/right: model E1/E2. Blue/black/red contour lines for positive/zero/negative densities. Contour interval 0.05 e Å^{-3}.

Bond-topological properties in the glucopyranosyl fragment may be compared with the monosaccharide fragments in sucrose, of which an experimental electron-density study was carried out recently (Jaradat *et al.*, 2007). For sucrose, $\rho(\mathbf{r}_{bcp})$/$\nabla^2\rho(\mathbf{r}_{bcp})$ values averaged over eight exocyclic C—O(H)

[1] Supplementary data for this paper are available from the IUCr electronic archives (Reference: SN5088). Services for accessing these data are described at the back of the journal.

Table 3
Average differences Δ of topological descriptors $\rho(\mathbf{r}_{bcp})$, $\nabla^2\rho(\mathbf{r}_{bcp})$ between experiment (models E1 and E2) and theory: B3LYP/6-311+G(d,p) (B); HF/6-311+G(d,p) (H) (Frisch *et al.*, 1998).

	$\Delta\rho(\mathbf{r}_{bcp})$ (e Å^{-3})	$\Delta\nabla^2\rho(\mathbf{r}_{bcp})$ (e Å^{-5})
E1–B	0.09	4.3
E1–H	0.08	9.5
E2–B	0.12	4.4
E2–H	0.11	9.0
H–B	0.054	5.5
E2–E1	0.045	2.0

bonds and ten C—C single bonds were derived as 1.90 (4) e Å^{-3}/−14.2 (15) e Å^{-5} and 1.76 (3) e Å^{-3}/−14.9 (6) e Å^{-5}. For bergenin, the corresponding quantities for three C—O(H) bonds are 1.87 (1) e Å^{-3}/−13.8 (6) e Å^{-5} and 1.83 (2) e Å^{-3}/−16.3 (5) e Å^{-5} for five C—C single bonds.

For the three six-membered rings in bergenin, the electron densities on the r.c.p.s are uniformly between 0.17 and 0.21 e Å^{-3}, and the corresponding Laplacian range is 2.7–3.0 e Å^{-5}. The r.c.p. in the glucopyranosyl ring of sucrose has $\rho(\mathbf{r}_{rcp})/\nabla^2\rho(\mathbf{r}_{rcp})$ = 0.14 e Å^{-3}/2.6 e Å^{-5}.

Bader's QTAIM theory also allows us to obtain atomic properties in terms of volumes and charges from integration over the zero-flux surfaces of the electron-density gradient-vector field. Since atomic volumes and charges are additive, the success of the integration procedure can easily be validated: The sum of atomic volumes in one unit cell should be equal to the experimental cell volume. Consequently, the sum of all atomic charges should add up to zero. For bergenin, the sum of atomic volumes (1491.3/1479.7 Å^3 for models E1/E2) differs by 0.1/0.7% from the experimental unit-cell volume V_{exp} = 1489.4 Å^3 (see Table 1), while the sum of charges differs by only 0.04/0.05 e from electroneutrality. The average difference between E1 and E2 charges and volumes is very small, 0.05 e and 0.26 Å^3, again within the normal spread of experimental error. For a detailed list of individual atomic properties, see the supplementary data.

In an attempt to derive a correlation between volumes and charges or other physical or chemical properties, two types of plots were generated (Figs. 4*a* and *b*). In Fig. 4(*a*) a charge *versus* volume diagram is displayed, which obviously does not show any correlation. This is in accordance with a corresponding diagram recently published for peptide fragments (Leherte *et al.*, 2007). Only a few clusters for the different elements and atom types can be recognized.

In Fig. 4(*b*) a plot of atomic volumes (only non-H atoms included) *versus* the sum of electronegativities (EN) of adjacent atoms shows some amount of linear correlation. We note that the strongest outlier is oxygen O3 being the acceptor of the only intramolecular hydrogen bond. If the donor hydrogen H1 were to be partly included in the EN sum of the nearest neighbors, the O3 data point would be shifted closer to the correlation line.

The H atoms, which are not included in the diagram of Fig. 4(*b*), can be easily distinguished whether they are bonded to carbon or oxygen (see the corresponding clusters in Fig. 4*a*). When bonded to the more electronegative oxygen, the H atoms lose volume and charge compared with H atoms bonded to carbon.

3.2. Hydrogen bonding and electrostatic potential

After the introduction of the aspherical invariom model, the H atoms closely approach positions normally found in neutron-diffraction experiments, see the summary in Table 4. This allows a more reliable analysis of hydrogen bonds.

As already mentioned, there are seven hydrogen bonds in the crystal structure of bergenin, according to the number of potential OH donors (Fig. 5). One of them (O4—H1···O3) is intramolecular, the other ones are intermolecular hydrogen bonds (Table 5). The strongest hydrogen bond is formed between the O6—H2 hydroxyl donor group and the water

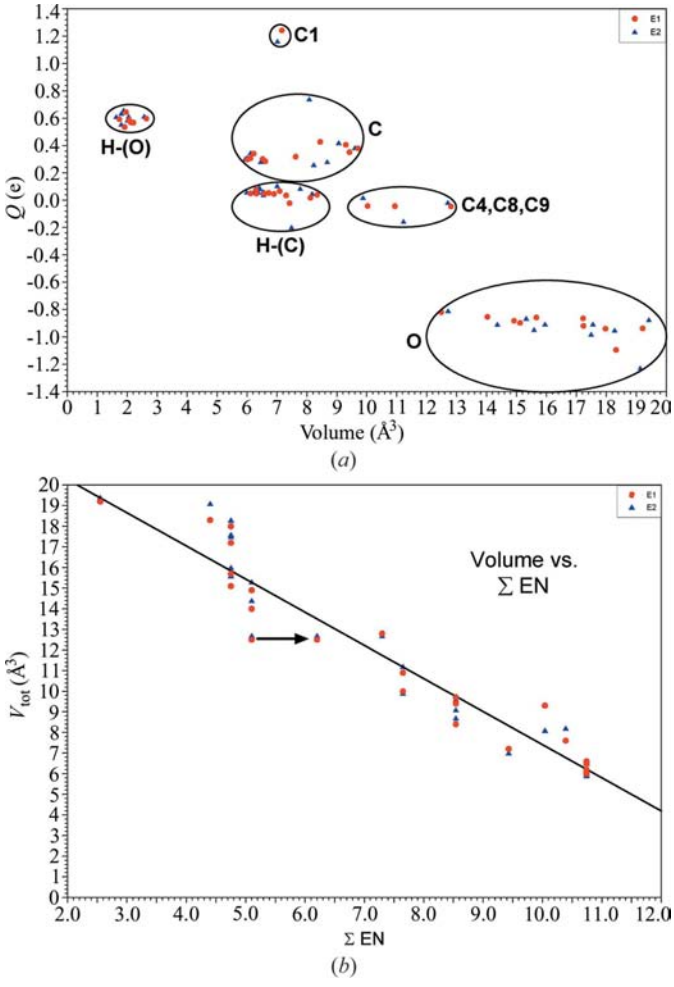

Figure 4
(*a*) Plot of Bader charges Q *versus* atomic basin volumes V_{tot}. Clusters according to atom types are marked. Red dots: model E1; blue triangles: model E2. (*b*) Representation of V_{tot} *versus* the sum of electronegativeties (EN) of adjacent atoms. The linear correlation coefficient is 0.96. The largest outlier (for O3) would approach closer to the least-squares line if the neighborhood of the hydrogen-bond donorship of H1 were considered in the EN summation (arrow, see also text).

Table 4
Averaged X—H bonds.

X—H	Spherical	Invariom (E1/E2)	Neutron[a]
O—H	0.86 (4)	0.93 (3)	0.97
C—H	0.96 (3)	1.08 (2)	1.06–1.09

References: (*a*) Allen *et al.* (1992).

oxygen O10 acceptor (see again the deformation-density distribution of this interaction, illustrated in Fig. 3, bottom).

The influence of hydrogen bonding on the electron density was studied quantitatively by means of topological properties, also listed in Table 5. In all cases, relatively low values of electron density and positive Laplacians at the b.c.p.s are indicative of closed-shell interactions (Koch & Popelier, 1995). Hydrogen-bond energies E_{HB} were calculated from the relation of Abramov (1997) which uses the electron-density $\rho(\mathbf{r}_{bcp})$ and Laplacian values $\nabla^2\rho(\mathbf{r}_{bcp})$ (see also Fig. 5), and from the relation of Espinosa (*et al.*, 1998), where only the hydrogen···acceptor distance (H···A) is entered. Since neither the $\rho(\mathbf{r}_{bcp})$ nor the $\nabla^2\rho(\mathbf{r}_{bcp})$ values differs strongly between the two experimental models E1 and E2, the Abramov hydrogen bonding energies are rather alike and their average difference is 1.2 kJ mol^{-1}. Accordingly the difference to the Espinosa hydrogen-bonding energy is small (2.0–2.5 kJ mol^{-1}) if the proper hydrogen positions of the invariom geometry are used. The hydrogen bond O6—H2···O10 is confirmed to be the strongest by E_{HB} > 60 kJ mol^{-1}, which is three times stronger than E_{HB} being close to 20 kJ mol^{-1} for the weakest hydrogen bond O9—H5···O6. Since the H···A distance is used in the Espinosa E_{HB} calculation, the spherical model would have led to lower hydrogen-bond energies, because shorter spherical O—H bond lengths (see Table 4) imply longer H···A acceptor distances and hence lower E_{HB}s. It follows that the invariom formalism promotes a more reliable derivation of quantitative hydrogen-bond properties in the Espinosa formalism. However, the E2 model obtained after multipole refinement obviously does not provide significantly more information about the intermolecular interactions in the bergenin lattice than the E1 model.

For the consideration of the reactive behavior of a chemical system, the three-dimensional distribution of its electrostatic potential is very helpful in that negative regions can be regarded as nucleophilic centers, whereas regions with positive electrostatic potential are potential electrophilic sites. The electrostatic potential, which can be derived directly from the electron density, was calculated from the experimental (E2) data using the method of Volkov, King *et al.* (2006) and is represented in Fig. 6 by a color code mapped on the isoelectron-density surface at $\rho(\mathbf{r})$ = 0.5 e Å^{-3}. The electrostatic potential makes the polarization of the electron density visible, in that, for example, a noticeable negative electrostatic potential is seen around the O atoms, while positive electrostatic potential regions are found around the H atoms. Moreover, it can be seen that the OH hydrogen atoms, which are involved in hydrogen bonding, have a stronger positive electrostatic potential than the H atoms bonded to the C atoms not being involved in such interactions (see the dark blue or deep violet and hence strong positive regions) so that in total the polarization in the hydrogen-bonding regions is visible.

While these features in the electrostatic potential already make intermolecular interactions visible, the sites and strengths of these types of contacts can also be studied from the illustration in Fig. 7, where the electron density is mapped on the Hirshfeld surface (Spackman & Byrom, 1997; McKinnon *et al.*, 1998) using a color code. It can easily be recognized from the intensity of the colored regions where hydrogen bonding takes place. The strongest electron-density

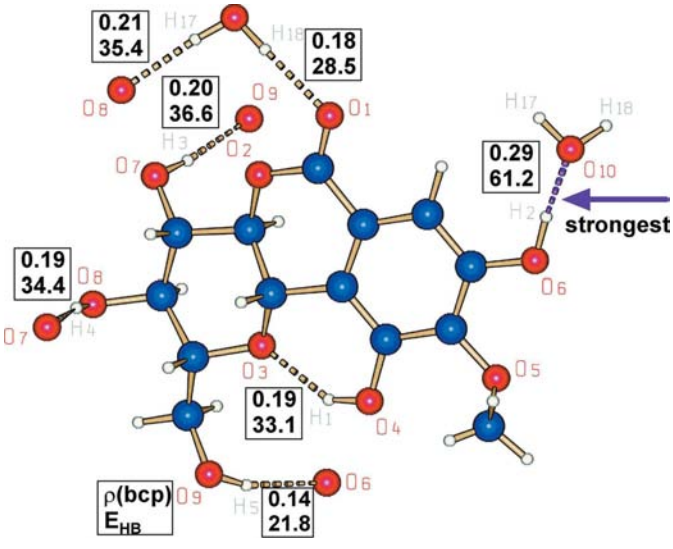

Figure 5
The seven hydrogen bonds in the crystal lattice of bergenin monohydrate. For each hydrogen bond, the value of the electron density (model E2) at the b.c.p. ($\rho(\mathbf{r}_{bcp})$, in e Å^{-3}) is given and the hydrogen-bond energy E_{HB} (in kJ mol^{-1}) after Abramov (1997).

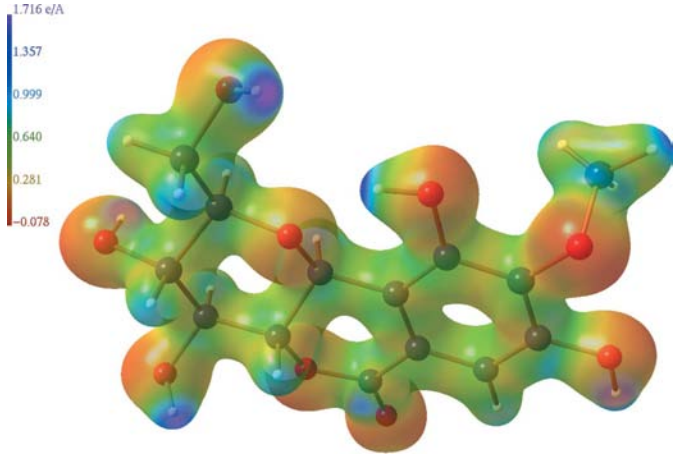

Figure 6
Experimental (E2) electrostatic potential, mapped by a color code (see color bar) on the electron-density isosurface at 0.5 e Å^{-3} (*MolIso* representation; Hübschle & Luger, 2006). For this isosurface value, the E1 model (not shown) looks alike within the graphical accuracy.

Table 5
Summary of hydrogen-bonding data (units in Å, °, e Å^{-3}, e Å^{-5}, kJ mol^{-1}).

D—H···A	D—H	H···A	D···A	D—H···A	$\rho(\mathbf{r}_{bcp})$	$\nabla^2\rho(\mathbf{r}_{bcp})$	E_{HB}†		E_{HB}‡
O4—H1···O3	0.91 (1)	1.87 (1)	2.666 (1)	145 (1)	0.19	3.03	30.16	21.81	33.40
					0.19	*2.97*			*33.13*
O6—H2···O10^{i}	0.98 (1)	1.65 (1)	2.620 (1)	171 (1)	0.29	4.73	66.59	46.46	61.22
					0.29	*4.72*			*61.17*
O7—H3···O9^{ii}	0.94 (1)	1.81 (1)	2.741 (1)	170 (1)	0.19	3.33	37.43	28.07	34.76
					0.20	*3.34*			*36.56*
O8—H4···O7^{iii}	0.92 (1)	1.82 (1)	2.737 (1)	172 (1)	0.19	3.32	34.83	30.16	34.71
					0.19	*3.26*			*34.44*
O9—H5···O6^{iv}	0.87 (1)	1.99 (1)	2.823 (1)	160 (1)	0.13	2.20	18.89	17.58	20.42
					0.14	*2.19*			*21.75*
O10—H17···O8^{iii}	0.92 (1)	1.84 (1)	2.764 (1)	175 (1)	0.20	2.80	33.60	24.30	34.11
					0.21	*2.69*			*35.42*
O10—H18···O1^{v}	0.94 (1)	1.92 (1)	2.857 (1)	175 (1)	0.16	2.35	25.19	25.19	25.42
					0.18	*2.32*			*28.48*

Symmetry codes: (i) $1-x,\frac{1}{2}+y,\frac{3}{2}-z$; (ii) $-1+x,y,z$; (iii) $\frac{1}{2}+x,\frac{1}{2}-y,1-z$; (iv) $\frac{1}{2}+x,\frac{3}{2}-y,1-z$; (v) $1+x,y,z$. † E_{HB} calculated after Espinosa's expression (Espinosa *et al.*, 1998), left column: H···A entered from geometry refinement after invariom transfer; right column: H···A entered from spherical geometry. ‡ E_{HB} calculated after Abramov's expression (Abramov, 1997). B.c.p. values and Abramov energies for model E1 in the first line, corresponding values for model E2 in italic in the second line.

region, indicated by the red circle (> 0.3 e Å^{-3}), indicates the site of the strongest hydrogen bond O6—H2···O10.

3.3. Assessment of invariom data: the test case sucrose

As already mentioned, the electron density of sucrose was recently determined based on a high-resolution ($\sin\theta/\lambda$ = 1.15 Å^{-1}) 20 K Mo $K\alpha$ data set (Jaradat *et al.*, 2007) followed by a full topological analysis according to Bader's AIM formalism. For an assessment of the invariom procedure applied to bergenin and the derived quantitative findings reported above, a room-temperature low-order data set of sucrose (Cu$K\alpha$, 2619 reflections, $\sin\theta/\lambda$ = 0.59 Å^{-1}) measured under comparable experimental conditions as for bergenin was used in an invariom refinement, so that the comparison of the resulting topological data with those of the high-resolution multipole-refined data published by Jaradat *et al.* (2007) could serve as a benchmark test for the reliability of the invariom formalism. The invariom bond-topological properties $\rho(\mathbf{r}_{bcp})$ and $\nabla^2\rho(\mathbf{r}_{bcp})$ and atomic volumes and charges were plotted *versus* the corresponding high-resolution multipole data (Figs. S1–S4, see supporting information) and can be summarized as follows: With few exceptions, the data points deviate from a bisecting line within an interval given by the recently introduced overall experimental transferability indices (Grabowsky *et al.*, 2009), which are 0.09 e Å^{-3} and 2.8 e Å^{-5} for $\rho(\mathbf{r}_{bcp})$ and $\nabla^2\rho(\mathbf{r}_{bcp})$ and 0.7 Å^3 and 0.11 e for volumes and charges. The exceptions are mainly seen for the atomic charges (the considered interval should be doubled), indicating a slightly less pronounced description of the polarization in the crystal by the invariom model. Hence, we are confident that invariom data are quantitatively reliable within the transferability indices given above.

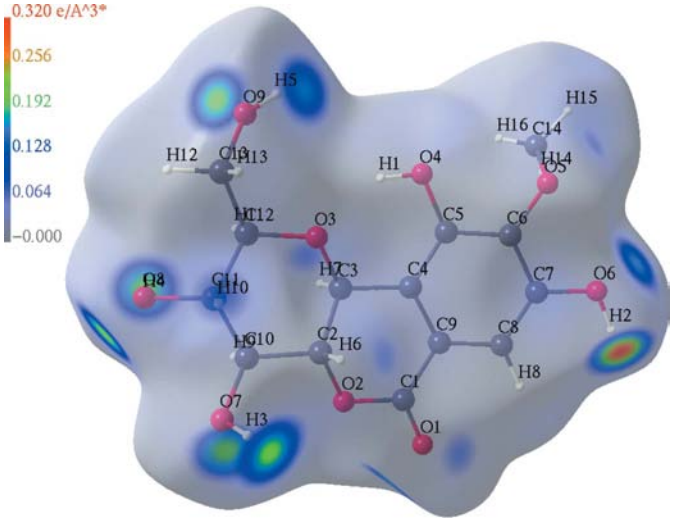

Figure 7
Electron-density (in e Å^{-3}) mapped on the Hirshfeld surface (Spackman & Byrom, 1997; McKinnon *et al.*, 1998) of bergenin. Illustration generated with *MolIso* (Hübschle & Luger, 2006).

4. Conclusion

This study has shown that simple X-ray diffraction experiments with inexpensive equipment combined with the software-supported invariom formalism can yield properties of the investigated chemical structure far beyond those obtainable from the IAM. The assignment of multipole populations from the invariom library has led to a molecular geometry with significantly improved hydrogen positions. It has also allowed sufficiently accurate ADPs to be obtained that are deconvolved from the electron-density distribution. Starting from the subsequently fixed positional and displacement parameters of the invariom model, a multipole refinement converges smoothly, although only a room-temperature low-resolution diffraction data set measured with Cu $K\alpha$ radiation was used. The reliability of the invariom results was confirmed by the quantitative findings for sucrose where invariom and high-resolution multipole data could be directly compared and found to be consistent with the recently published transferability indices.

It holds for the experimental E1 and E2 models that in addition to intramolecular topological descriptors, intermolecular electronic properties can be derived which are highly useful, especially for biologically active compounds. Drug–receptor interactions of such compounds are often not only directed by steric and van der Waals interactions, but also by complementarity in their electronic properties. Hence, an intermolecular electron-density distribution can provide further information for the understanding of such interactions on an atomic level.

Regarding these aspects, the invariom formalism is properly suited for further application not only in traditional medicine, which is frequently part of the public health system (Luger *et al.*, 2000; Kingsford-Adaboh *et al.*, 2001, 2006), but also as an affordable tool in general drug research.

Support of this work is gratefully accepted from the DFG within the special priority program SPP 1178, grant Lu 222/29-2, an Emmy-Noether research fellowship, Di 921/3-1 and within the Graduate School 788 (Hydrogen Bonding and Hydrogen Transfer). We thank Dr Tran Dinh Thang, Vinh University, Vietnam, for a crystalline sample of bergenin.

References

Abramov, Yu. A. (1997). *Acta Cryst.* A**53**, 264–272.
Allen, F. H. (2002). *Acta Cryst.* B**58**, 380–388.
Allen, F. H., Kennard, O., Watson, D. G., Brammer, L., Orpen, A. G. & Taylor, R. (1992). *International Tables for X-ray Crystallography*, Vol. C, ch. 9.5, pp. 685–706. Amsterdam: Kluwer Academic Publishers.
Bader, R. F. W. (1994). *Atoms in Molecules. A Quantum Theory*, 2nd ed. Oxford: Clarendon Press.
Biegler-König, F. (2001). *J. Comput. Chem.* **22**, 545–559.
Burnett, M. N. & Johnson, C. K. (1996). *ORTEP*III, Report ORNL-6895. Oak Ridge National Laboratory, Tennessee, USA.
Caldas, C. S., De Simone, C. A., Pereira, M. A., Malta, V. R. S., Carvalho, R. L. P., Da Silva, T. B. C., Sant'ana, A. E. G. & Conserva, L. M. (2002). *Acta Cryst.* E**58**, o609–o611.
Dittrich, B., Hübschle, C. B., Holstein, J. & Fabbiani, F. P. A. (2009). *J. Appl. Cryst.* **42**, 1020–1029.
Dittrich, B., Hübschle, C. B., Messerschmidt, M., Kalinowski, R., Girnt, D. & Luger, P. (2005). *Acta Cryst.* A**61**, 314–320.
Dittrich, B., Koritsánszky, T., Grosche, M., Scherer, W., Flaig, R., Wagner, A., Krane, H.-G., Kessler, H., Riemer, C., Schreurs, A. M. M. & Luger, P. (2002). *Acta Cryst.* B**58**, 721–727.
Dittrich, B., Koritsánszky, T. & Luger, P. (2004). *Angew. Chem. Int. Ed.* **43**, 2718–2721.
Dittrich, B., McKinnon, J. J. & Warren, J. E. (2008). *Acta Cryst.* B**64**, 750–759.
Dominiak, P. M., Volkov, A., Li, X., Messerschmidt, M. & Coppens, P. (2007). *J Chem. Theory Comput.* **3**, 232–247.
Espinosa, E., Molins, E. & Lecomte, C. (1998). *Chem. Phys. Lett.* **285**, 170–173.
Frick, W., Hofmann, J., Fischer, H. & Schmidt, R. (1991). *Carbohydr. Res.* **210**, 71–77.
Frisch, M. J. *et al.* (1998). *GAUSSIAN*98, Revision A.7. Gaussian Inc., Pittsburgh PA, USA.
Grabowsky, S., Kalinowski, R., Weber, M., Förster, D., Paulmann, C. & Luger, P. (2009). *Acta Cryst.* B**65**, 488–501.
Hansen, N. K. & Coppens, P. (1978). *Acta Cryst.* A**34**, 909–921.
Hofmann, A., Kalinowski, R., Luger, P. & van Smaalen, S. (2007). *Acta Cryst.* B**63**, 633–643.
Hofmann, A., Netzel, J. & van Smaalen, S. (2007). *Acta Cryst.* B**63**, 285–295.
Hübschle, C. B. & Luger, P. (2006). *J. Appl. Cryst.* **39**, 901–904.
Hübschle, C. B., Luger, P. & Dittrich, B. (2007). *J. Appl. Cryst.* **40**, 623–627.
Jaradat, D. M. M., Mebs, S., Checinska, L. & Luger, P. (2007). *Carbohydr. Res.* **352**, 1480–1489.
Kingsford-Adaboh, R., Dittrich, B., Hübschle, C. B., Gbewonyo, W. S. K., Okamoto, H., Kimura, M. & Ishida, H. (2006). *Acta Cryst.* B**62**, 843–849.
Kingsford-Adaboh, R., Osei-Fosu, P., Asomaning, W., Weber, M. & Luger, P. (2001). *Cryst. Res. Tech.* **36**, 107–115.
Koch, U. & Popelier, P. L. A. (1995). *J. Phys. Chem.* **99**, 9747–9754.
Leherte, L., Guillot, B., Vercauteren, D., Pichon-Pesme, V., Jelsch, C., Lagoutte, A. & Lecomte, C. (2007). *The Quantum Theory of Atoms in Molecules*, edited by C. F. Matta & R. J. Boyd, ch. 11, pp. 285–315. Weinheim: Wiley-VCH.
Luger, P. (2007). *Org. Biomol. Chem.* **5**, 2529–2540.
Luger, P., Weber, M., Dung, N., Ngoc, P., Tuong, D. & Rang, D. (2000). *Cryst. Res. Tech.* **35**, 355–362.
McKinnon, J. J., Mitchell, A. S. & Spackman, M. A. (1998). *Chem. Eur. J.* **4**, 2136–2141.
Messerschmidt, M., Scheins, S. & Luger, P. (2005). *Acta Cryst.* B**61**, 115–121.
Netzel, J., Hoffmann, A. & van Smaalen, S. (2008). *CrystEngComm*, **10**, 335–343.
Pichon-Pesme, V., Lecomte, C. & Lachekar, H. (1995). *J. Phys. Chem.* **99**, 6242–6250.
Shang-Zhen, Z., Hua, Y. J., Xu-Wei, S., Zhong-Yuan, Z. & Guo-Zhi, H. (1989). *J. Struct. Chem.* **8**, 305–310.
Sheldrick, G. M. (2008). *Acta Cryst.* A**64**, 112–122.
Smaalen, S. van, Palatinus, L. & Schneider, M. (2003). *Acta Cryst.* A**59**, 459–469.
Spackman, M. A. & Byrom, P. G. (1997). *Chem. Phys. Lett.* **267**, 215.
Stewart, R. F. (1976). *Acta Cryst.* A**32**, 565–574.
Volkov, A., King, H. F., Coppens, P. & Farrugia, L. J. (2006). *Acta Cryst.* A**62**, 400–408.
Volkov, A., Macchi, P., Farrugia, L. J., Gatti, C., Mallinson, P. R., Richter, T. & Koritsanszky, T. (2006). *XD*2006. University at Buffalo, NY, USA; University of Milano, Italy; University of Glasgow, UK; CNRISTM, Milano, Italy; Middle Tennessee State University, TN, USA.
Ye, Y.-P., Sun, H.-X. & Pan, Y.-J. (2004). *Acta Cryst.* C**60**, o397–o398.
Zarychta, B., Pichon-Pesme, V., Guillot, B., Lecomte, C. & Jelsch, C. (2007). *Acta Cryst.* A**63**, 108–125.